Stochastic Inverse-Compton Scattering Strongly Modifies the Electron and Positron Fluxes From Pulsars and Dark Matter

Isabelle John[a,*] **and Tim Linden**[a]

[a]*Stockholm University and The Oskar Klein Centre for Cosmoparticle Physics, Alba Nova, 10691 Stockholm, Sweden*

E-mail: isabelle.john@fysik.su.se, linden@fysik.su.se

High-energy cosmic-ray electrons and positrons cool rapidly as they propagate through the Galaxy, due to synchrotron interactions with magnetic fields and inverse-Compton scattering interactions with photons of the interstellar radiation field. Typically, these energy losses have been modelled as a continuous process. However, inverse-Compton scattering is a stochastic process, characterised by interactions that are rare and catastrophic. In this work, we take the stochasticity of inverse-Compton scattering into account and calculate the contributions to the local electron and positron fluxes from different sources. Compared to the continuous approximation, we find significant changes: for pulsars, which produce electron-positron pairs as they spin down, the spectrum becomes significantly smoother. For TeV-scale dark matter particles, which annihilate into electrons and positrons, the signal becomes strongly enhanced around the energy corresponding to the dark matter mass. Combined, these effects significantly improve our ability to use spectral signatures in the local electron and positron spectra to search for particle dark matter at TeV energies.

*Speaker

1. Introduction

The local cosmic-ray electron and positron (hereafter $e^{\pm}$) fluxes have been measured to great precision (e.g. [1, 2]), but their origin is not fully understood. Observations suggest that pulsars produce highly energetic $e^{\pm}$ that dominate the positron flux at high energies (e.g. [3–5]). Another contribution could come from annihilating dark matter particles that would show a signal with a sharp cutoff corresponding to the dark matter mass (e.g. [6–9]).

In order to predict the $e^{\pm}$ contribution from different sources to the local $e^{\pm}$ flux, energy losses during their propagation through the Galaxy must be modelled properly. The two relevant energy loss processes at high energies are synchrotron interactions due to Galactic magnetic fields and inverse-Compton scattering (ICS) interactions, where a high-energy $e^{\pm}$ interacts with and transfers some fraction of its energy to a lower energy photon of the interstellar radiation field (ISRF). Typically, these energy losses have been treated as a continuous process over time. While this approximation holds well for synchrotron losses, ICS is a highly stochastic process where energy loss events are rare and can be catastrophic, removing a large fraction of the $e^{\pm}$ at once.

In this work, we show that if the stochasticity of ICS is correctly taken into account instead of approximating the energy losses by a continuous model, the expected spectral signals from pulsars and dark matter are significantly changed. For pulsars, the feature remains much smoother [10]. For dark matter, the cutoff at the dark matter mass is enhanced [11]. This relaxes a possible degeneracy between the expected signals from these two types of sources introduced by the continuous approximation.

2. Methodology

The energy loss rate for synchrotron radiation is given by

$$\frac{dE_e}{dt} = \frac{4}{3}\sigma_T c \left(\frac{E_e}{m_e}\right) u_B, \tag{1}$$

where u_B is the energy density of the magnetic field (calculated from the magnetic field strength (in units of G) by $u_B = B^2/(8\pi) \times 6.24 \times 10^{11}$ eV/cm^3), σ_T is the Thomson cross section and c the speed of light. The average energy loss in a synchrotron interaction is calculated by

$$E_{\text{sync}} = \frac{3\gamma^2 eB}{4\pi m_e c} \approx 0.06 \left(\frac{B}{1\,\mu\text{G}}\right)\left(\frac{E_e}{1\,\text{TeV}}\right)^2 \text{eV}. \tag{2}$$

For example, for a typical magnetic field strength of $B = 3\,\mu$G and $e^{\pm}$ energy of $E_e = 300$ TeV, the average energy loss in an interaction is 16 keV, which is only a small fraction of the $e^{\pm}$ energy. Additionally, synchrotron interactions happen frequently. This makes Equation 1, that treats synchrotron losses as continuous process, a reasonable approximation.

For ICS, the interaction cross section is given by [12–14]:

$$\frac{d^2\sigma(E_\gamma, \theta)}{d\Omega dE_\gamma} = \frac{r_0^2}{2\nu_i E_e^2} \times \left[1 + \frac{z^2}{2(1-z)} - \frac{2z}{b_\theta(1-z)} + \frac{2z^2}{b_\theta^2(1-z)^2}\right] \tag{3}$$

where ν_i is the initial energy of the ISRF photon, E_γ is energy of the outgoing γ-ray photon, θ the scattering angle, r_0 the classical electron radius, $z \equiv E_\gamma/E_e$ and $b_\theta \equiv 2(1 - \cos\theta)\nu_i E_e$. The total energy loss rate for ICS is then given by [15]

$$\frac{dE_e}{dt} = \frac{12c\sigma_T}{m_e^2}E_e^2 \int_0^\infty \nu n\,(\nu)\,J\,(\Gamma)\;d\nu,\tag{4}$$

where σ_T is the Thomson cross section, $\gamma = E_e/m_e$, $n(\nu)$ is the energy spectrum of the ISRF photons. $J\,(\Gamma)$ takes into account the suppression of the Thomson cross-section due to Klein-Nishina effects, which decreases the cross section at high $e^\pm$ and photon energies due to kinematics. It is given by

$$J\,(\Gamma) = \int_0^1 \frac{qG\,(q,\Gamma)}{(1+\Gamma q)^3},\tag{5}$$

where $\Gamma = 4\nu\gamma/m_e$ and $q = \nu_s/(\Gamma(\gamma m - \nu_s))$, where ν_s is the energy of the scattered γ-ray photon. The function $G(q,\Gamma)$ is given by

$$G\,(q,\Gamma) = 2q \ln q + (1 + 2q)(1 - q) + \frac{\Gamma^2 q^2(1 - q)}{2\,(1 + \Gamma q)}.\tag{6}$$

This means that, for interactions at high $e^\pm$ and ISRF photon energies ($\nu_i E_e > m_e^2$), ICS interactions are especially rare, and can remove a large fraction of the $e^\pm$ in a single interaction. For example, for a 100 TeV $e^\pm$ and a photon of the cosmic microwave background of $\sim 10^{-3}$ eV, the average energy loss is ~ 50 TeV, and becomes even larger for higher photon energies. This shows that ICS is a highly stochastic process, where interactions are increasingly rare at high energies, and the energy lost in a single interaction can vary strongly.

2.1 Continuous Energy Loss Model

Energy losses are commonly modelled as a continuous process. We use Equations 1 and 4 to calculate the energy loss rates for synchrotron and ICS processes, choosing an appropriately small time step that removes the corresponding amount of energy from the $e^\pm$ in each step. We repeat this process until the $e^\pm$ have cooled for the duration of interest.

2.2 Stochastic Energy Loss Model

In the stochastic energy loss model, we treat ICS as a stochastic process, while maintaining the continuous treatment for the synchrotron losses as discussed above. For ICS, we apply Equations 3 to 6.

To take the stochasticity of ICS into account, we set up a Monte Carlo code and perform the following steps: (1) An $e^\pm$ is injected at some initial energy. (2) Choosing a time step that is sufficiently small so that the probability of having two ICS interactions in a single time step is negligible, we use a Monte Carlo setup to determine if an ICS interaction happens in that time step, and at what photon energy. (3) If an ICS interaction happened, we use another Monte Carlo to determine how much energy is transferred from the $e^\pm$ to the photon, i.e. the energy loss. (4) We remove energy losses from ICS and synchrotron interactions to calculate the new $e^\pm$ for the next iteration, and repeat this process until the desired cooling time is reached.

2.3 Pulsar Modelling

Pulsars are rapidly rotating neutron stars that convert some fraction of their spindown power into highly energetic $e^\pm$ pairs, following

$$\frac{dN}{dE_e} = Q(t)E_e^{-\alpha} \exp\left(\frac{E_e}{E_{\text{cut}}}\right), \tag{7}$$

where α is the spectral index and E_{cut} is the cutoff energy of the power law, which reduces the number of $e^\pm$ injected above this energy. $Q(t)$ is a normalisation term that takes into account the energy-dependence of the $e^\pm$ injection, i.e. as the pulsar ages and spins more slowly, it converts less energy into $e^\pm$ pairs. This is given by

$$L(t) = \eta L_0 \left(1 + \frac{t}{\tau}\right)^{-2}, \tag{8}$$

where L and L_0 are the current and initial pulsar luminosity, t is the pulsar age and τ is the spindown time scale. The efficiency of how much spindown power is converted to $e^\pm$ is given by η.

The exact parameters are individual for a pulsar. Here we choose the pulsar Geminga as a template system, as it is a pulsar that is expected to strongly contribute to the $e^\pm$ flux. It is middle-aged (342 kyr old) and nearby, 250 pc. Best fit parameters suggest an injection spectrum with $\alpha = 1.9$, $E_{\text{cut}} = 100$ TeV, $\tau = 9100$ yr , with a total energy output of 9.8×10^{50} GeV (i.e. energy output from age 0 until now $E_{\text{tot}} = \int_0^{342} L(t)dt$), and an efficiency of $\eta = 0.1$.

We assume a standard value for the magnetic field strength of 3 μG and an ISRF corresponding to 4 components: the cosmic-microwave background (energy density $u = 0.26$ eV/cm^3, temperature $T = 2.7$ K), infrared ($u = 0.60$ eV/cm^3, $T = 20$ K), optical ($u = 0.60$ eV/cm^3, $T = 5000$ K) and ultra-violet ($u = 0.10$ eV/cm^3, $T = 20000$ K) [5]. For the continuous model, the pulsar is modelled following an analytic model from [3].

2.4 Dark Matter Modelling

For dark matter annihilations into $e^\pm$ pairs, the $e^\pm$ are injected at a single energy corresponding to the dark matter mass. Since dark matter particles annihilate continuously, we inject them according to a uniform distribution over time. The rate of $e^\pm$ production from dark matter annihilations is given by

$$\frac{dn_e}{dt} = \frac{1}{2}\left(\frac{\rho_0}{m_{\text{DM}}}\right)^2 \langle \sigma v \rangle \frac{dN_e}{dE_e}, \tag{9}$$

where n_e is the number density of $e^\pm$, ρ_0 the local dark matter energy density, m_{DM} the mass of the dark matter particle, $\langle \sigma v \rangle$ the thermally averaged dark matter annihilation cross section, and dN_e/dE_e is the energy injection spectrum of $e^\pm$. After taking energy losses account, the $e^\pm$ flux at Earth is

$$\Phi_e = \frac{c}{4\pi} n_e. \tag{10}$$

We consider dark matter masses at 10 TeV, 30 TeV, 50 TeV, 100 TeV and 300 TeV. For synchrotron losses we choose several magnetic field strengths that are within known uncertainties,
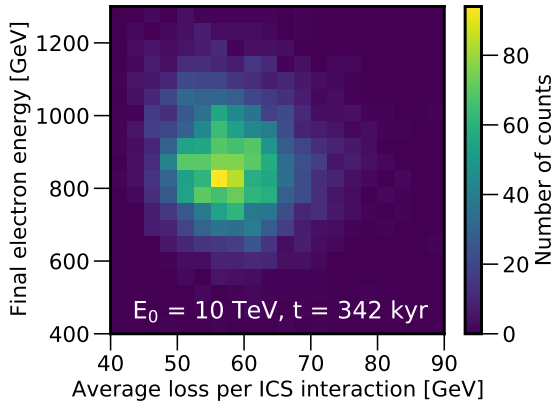
Figure 1: The average energy lost in an ICS interaction and the distribution of final $e^\pm$ energies for $e^\pm$ injected at 10 TeV and a cooling time of 342 kyr for stochastic ICS.
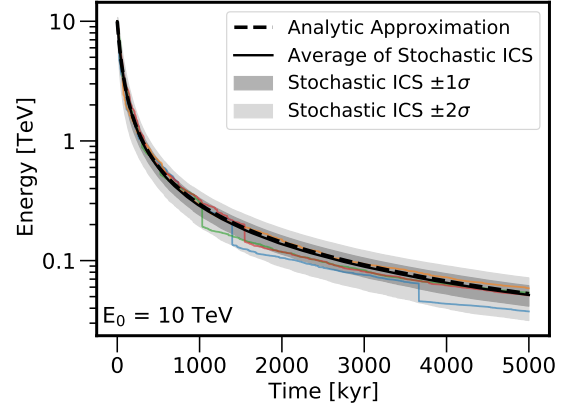
Figure 2: The $e^\pm$ energy evolution over 5 Myr. Solid lines represent the stochastic ICS model, where the black line shows the average. The gray shaded bands show the 1σ and 2σ spread respectively. The continuous result is given in dashed.

since the exact magnetic field strength is not known, and to study the impact of synchrotron losses, that dominate over ICS losses at a few hundreds of TeV. We choose the values 1, 2 and 3 μG.

3. Results

3.1 Pulsar Spectrum

Figures 1 and 2 illustrate the effect of the stochasticity of ICS on the $e^\pm$ energies: $e^\pm$ are simulated starting at the same initial energy (10 TeV) and cool for the same amount of time.

Figure 1 shows the average energy lost in an ICS interaction and the final distribution of $e^\pm$ energies, showing a spread of about 40–50%. On average, each $e^\pm$ only undergoes 110 ICS interactions in 342 kyr. Figure 2 shows the energy evolution over time. Even after 5 Myr, the distribution in final energies is about 40% at 1σ. Note that in the continuous model, all $e^\pm$ cool to the same final energy.

Figure 3 shows the pulsar spectrum. Since high energy $e^\pm$ lose energy faster than lower energy $e^\pm$, $e^\pm$ cool down to the same energy, resulting in a sharp cutoff in the $e^\pm$ flux. This feature corresponds to the pulsar age – as the pulsar becomes older, these $e^\pm$ have more time to cool to the same decreasing energy. Therefore, in the continuous model (blue), the pulsar spectrum shows
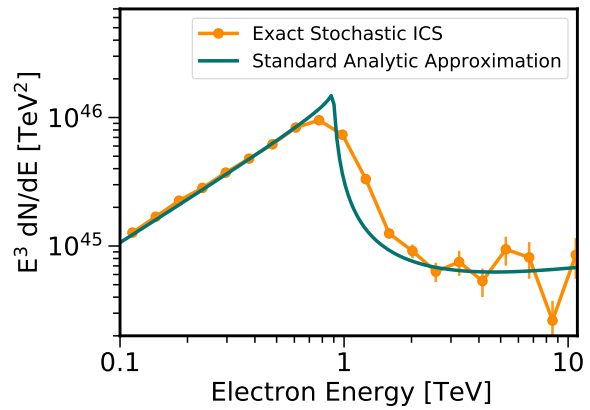
Figure 3: The contribution to the $e^\pm$ flux from a pulsar in the continuous model (blue) and stochastic model (orange), where the stochastic contribution is smoother by about 50% compared to the continuous model.
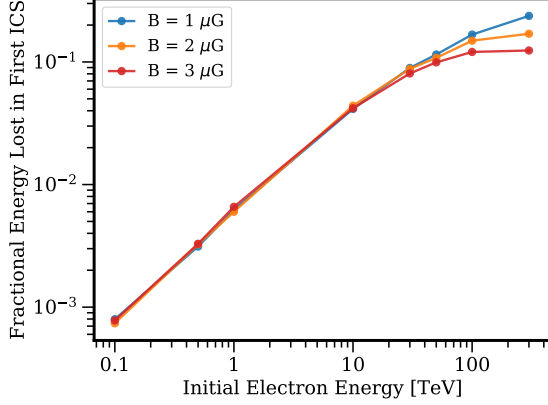
Figure 4: The fractional energy lost in the first ICS interaction at TeV energies. The energy lost increases with increasing initial energy.
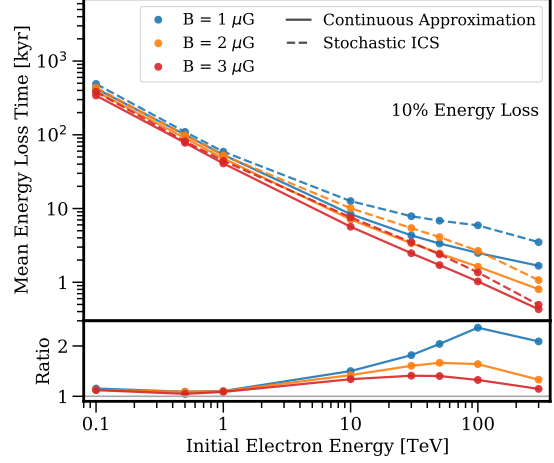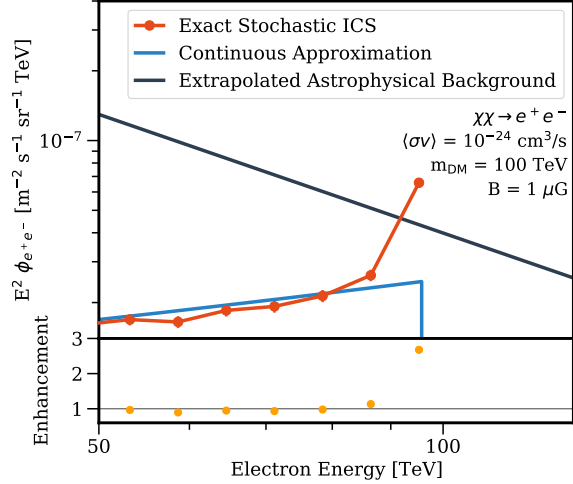

Figure 5: The mean time until 10% of the initial energy are lost in the continuous (solid) and stochastic (dashed) model. Since ICS interactions are suppressed at high energies, the mean energy loss time is significantly longer in the stochastic model.

a sharp cutoff. However, this sharp feature is prevented from building up in the stochastic model (orange) since the $e^{\pm}$ cool to a range of energies rather than a single value. This results in the cutoff being smeared out by about 50% compared to the continuous model.

3.2 Dark Matter Spectrum

Figure 4 shows the fractional energy lost in the first ICS interaction for TeV-scale energies and different magnetic field models. At 100 TeV, the average energy lost is 10%, which is a significant fraction of the $e^{\pm}$ energy. Figure 5 shows the mean time it takes to lose 10% of the initial energy for the continuous model (solid lines) and stochastic model (dashed lines). In the stochastic case, the energy loss time is longer since interactions are suppressed at high energies, while this is not taken into account by the continuous model, where energy is removed from the $e^{\pm}$ immediately. Consequently, this affects the dark matter signal as shown in Figure 6: the signal of a 100 TeV dark matter particle with the continuous model (blue) and the

Figure 6: The $e^{\pm}$ flux for a dark matter mass of 100 TeV. The cutoff in the continuous model (blue) is enhanced by a factor of 2.6 in the stochastic model (red).

stochastic model (red), where the stochastic model shows a strong enhancement of about a factor
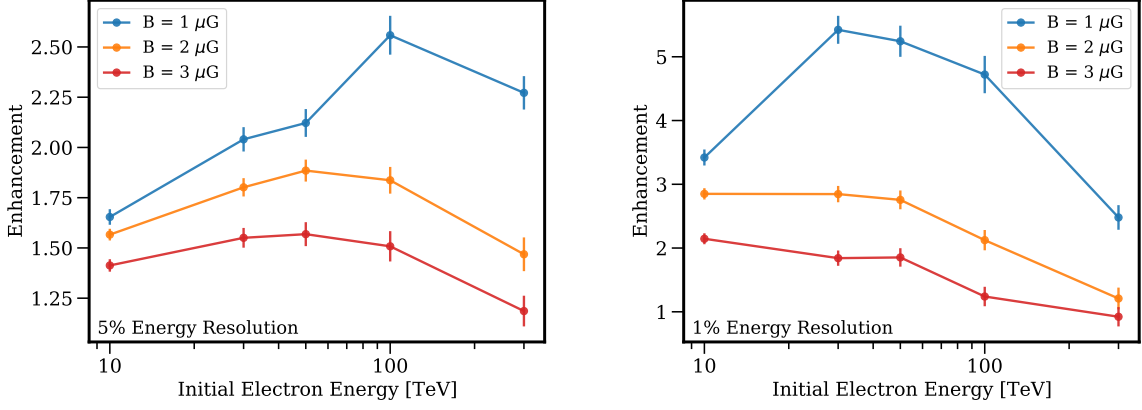
Figure 7: The enhancement across dark matter masses and magnetic field models for an energy resolution of 5% (left) and 1% (right). The enhancement increases with better resolution.

of 2.6 in the cutoff at the dark matter mass compared to the continuous model. Similar results for different dark matter masses and magnetic field models can be found in [11]. We note that the enhancement depends on the energy resolution – at 100 TeV, the average energy lost in the first ICS interaction takes about 10%, meaning that an energy resolution of 5% resolves the feature sufficiently well. At lower energies, the fractional energy lost in the first ICS interaction decreases, see Figure 4. To compensate for this, a higher energy resolution is required. This is illustrated in Figure 7 that shows the enhancement of the feature for different dark matter masses and magnetic field models for a 5% and 1% energy resolution, respectively. Since an energy resolution of 5% at 100s of TeV is realistic for upcoming experiments (e.g. CTA [16]), we choose to focus on TeV-scales, where this resolution is sufficient so that experimental searches can benefit from the enhanced feature and the detectability of dark matter signals in the $e^{\pm}$ is increased.

Notably, the stochastic treatment of ICS results in a smoothing effect for pulsars and in a sharpening effect in dark matter. To understand these opposing effects better, one has to consider the energy- and time-dependence of the injection of the two source types. Pulsars create $e^{\pm}$ at a range of energies, but inject most of them in a very short amount of time, close to a burst-like injection. On the other hand, dark matter particles create $e^{\pm}$ at a single energy, corresponding to the dark matter mass, but inject them continuously over time, as dark matter particles continuously annihilate. This results in the different effects of stochastic ICS on pulsar and dark matter contributions.

4. Discussion and Conclusion

We show that if inverse-Compton scattering energy losses are treated using an accurate stochastic model instead of the continuous approximation, the expected contribution from pulsars and dark matter to the local cosmic-ray $e^{\pm}$ fluxes change. For pulsars, the contribution becomes smoother. While the continuous models predict sharp features and thus generally require a large number of pulsars to fit the smooth positron flux, our result re-introduces the possibility of just a small number of dominant sources. For dark matter, the spectral cutoff is strongly enhanced. This increases the detectability in upcoming and future experiments, such as CTA [16], AMS-100 [17] and HERD [18].

Combined, these effects solve the potential degeneracy of pulsar and dark matter features in the $e^{\pm}$ flux and increase the distinguishability of pulsar and dark matter contributions in the local $e^{\pm}$ fluxes. Most importantly, these results re-establish dark matter as the only known astrophysical mechanisms that can introduce sharp spectral features in the local cosmic-ray $e^{\pm}$ fluxes.

References

[1] O. Adriani, G. C. Barbarino, G. A. Bazilevskaya, R. Bellotti, M. Boezio, E. A. Bogomolov, L. Bonechi, M. Bongi, and PAMELA Collaboration, PRL **105**, 121101 (2010), arXiv:1007.0821 [astro-ph.HE] .

[2] AMS-02 Collaboration (AMS Collaboration), Phys. Rev. Lett. **113**, 121101 (2014).

[3] D. Hooper, P. Blasi, and P. D. Serpico, JCAP **01**, 025 (2009), arXiv:0810.1527 [astro-ph] .

[4] A. U. Abeysekara *et al.* (HAWC), Science **358**, 911 (2017), arXiv:1711.06223 [astro-ph.HE] .

[5] D. Hooper, I. Cholis, T. Linden, and K. Fang, Phys. Rev. D **96**, 103013 (2017), arXiv:1702.08436 [astro-ph.HE] .

[6] N. Arkani-Hamed, D. P. Finkbeiner, T. R. Slatyer, and N. Weiner, Phys. Rev. D **79**, 015014 (2009), arXiv:0810.0713 [hep-ph] .

[7] L. Bergstrom, T. Bringmann, I. Cholis, D. Hooper, and C. Weniger, Phys. Rev. Lett. **111**, 171101 (2013), arXiv:1306.3983 [astro-ph.HE] .

[8] I. John and T. Linden, JCAP **12**, 007 (2021), arXiv:2107.10261 [astro-ph.HE] .

[9] A. Coogan, B. V. Lehmann, and S. Profumo, JCAP **10**, 063 (2019), arXiv:1903.07177 [astro-ph.HE] .

[10] I. John and T. Linden, Phys. Rev. D **107**, 103021 (2023), arXiv:2206.04699 [astro-ph.HE] .

[11] I. John and T. Linden, (2023), arXiv:2304.07317 [hep-ph] .

[12] O. Klein and Y. Nishina, Nature **122**, 398 (1928).

[13] G. R. Blumenthal and R. J. Gould, Rev. Mod. Phys. **42**, 237 (1970).

[14] F. A. Aharonian and A. M. Atoyan, Ap&SS **79**, 321 (1981).

[15] Schlickeiser and Ruppel, New J. Phys. **12**, 033044 (2010), arXiv:0908.2183 [astro-ph.HE] .

[16] G. Maier, L. Arrabito, K. Bernlöhr, J. Bregeon, P. Cumani, T. Hassan, J. Hinton, and A. Moralejo, "Performance of the cherenkov telescope array," (2019), arXiv:1907.08171 [astro-ph.IM] .

[17] S. Schael *et al.*, Nucl. Instrum. Meth. A **944**, 162561 (2019), arXiv:1907.04168 [astro-ph.IM] .

[18] S. N. Zhang *et al.* (HERD), Proc. SPIE Int. Soc. Opt. Eng. **9144**, 91440X (2014), arXiv:1407.4866 [astro-ph.IM] .